

Quantum eigenvalues and eigenfunctions of an electron confined between conducting planes

Don MacMillen  ¹

¹*San Mateo, California*^{*}

(Dated: January 21, 2026)

Two of the most iconic systems of quantum physics are the particle in a box and the Coulomb potential (the third is, of course, the harmonic oscillator). In this expository paper, we consider the quantum solution to the problem of an electron confined between the grounded planes of an infinite capacitor. The potential arises from the image charges that form in the grounded planes, along with the added condition that at $x = 0, L$, where L is the distance between the planes, the wavefunction must be zero. This effectively couples a hydrogen like system to a particle-in-a-box (PIB) based on L , the distance between the planes. The problem of finding the electrostatic potential of this infinite series of image charges is an old one, going back to at least 1929 [1]. Here, we give a short derivation for one of the limiting cases that yields a compact expression and show how the Kellogg infinite summation formula converges to that value. We note here that this potential is a symmetric double well potential, so there will be many familiar properties of its solutions. Then using that potential, we solve Schrödinger's equation using a spectral technique. The limiting forms of a particle in a box for small L (and high E), and that of a (degenerate) bound image charge [2] [3] at large L and small energy are recovered. We also discuss the tunneling level splitting that occurs in the transition from the large L to the small L regime.

I. INTRODUCTION

Confined quantum systems have long been the subject of various studies [4] [5]. Here we consider the quantum solution to the problem of an electron confined between the grounded planes of an infinite capacitor. To solve that quantum problem we need the potential of the electron in that configuration. This electrostatic problem of finding that potential is an old one. While it is not explicitly in Maxwell's "A Treatise on Electricity and Magnetism" it is perhaps implicitly contained in the problem of image charges in the presence of a conducting sphere, when the radius is allowed to go to infinity [6] [7].

In 1929 Kellogg [1] considers the problem of calculating the potential at any location (x, y, z) in the space between two parallel conducting planes where a unit charge is located at $(c, 0, 0)$ with $0 < c < L$. Table I illustrates the convergence of the truncated image-charge series toward the closed-form result in Eq. (6).

In a series of papers by different authors, and largely appearing in the American Journal of Physics, the problem of computing the charge distribution on the two plates is considered. Wong and Kittel [8] develop a series solution to this problem, utilizing results from J.D. Jackson [9]. They also develop a different series solution for the potential far from the charge that has better convergence properties than the original Kellogg summation.

Pumplin [10] obtains Green's function, again using the method of images, and then uses a Sommerfeld-Watson transform to obtain an integral representation for the potential. He then derives an asymptotic expression for

the potential, which is found to fall off exponentially. A very interesting result that shows that the two planes are very effective in screening a charge that is placed between them.

Glasser [11] then simplifies Pumplin's results and obtains a closed form solution along a line that passes directly through the charge. This is not exactly the potential that we seek, but it is noteable in that it results in an expression with two digamma functions, which we will see again shortly.

Interest in the problem of the potential and surface charge density in this constrained system continued through to the present day [12] [13] [14] [15] [16]. Concepts developed by the early set of papers in the American Journal of Physics continue to be relevant to problems in bilayer graphene [17] and in scanning quantum dot microscopy [18]. Further applications of these ideas have played a role in image induced surfaces states [19] and in 2D materials [20]. We expect that these confined quantum systems to continue to be of interest and find new applications.

In what follows, we first develop a closed form of the potential that an electron experiences when confined between two conduction planes and examine its form. Then we utilize a spectral method to solve this confined system to yield both the energies and states of the system. Next, we present the results of the solves and discuss E as a function of L , the approach of $E(n)$ to $\frac{1}{2}(\frac{\pi n}{L})^2$ for small L and to $-\frac{1}{32n^2}$ in the large L regime.

* don.macmillen@gmail.com

II. THE IMAGE POTENTIAL

We start with the series solution given by Kellogg on page 230 [1]:

$$U = \sum_{n=-\infty}^{\infty} e \left(\frac{1}{\sqrt{(x - 2nL - c)^2 + y^2 + z^2}} - \frac{1}{\sqrt{(x - 2nL + c)^2 + y^2 + z^2}} \right). \quad (1)$$

This equation pairs image charges of opposite sign that differ by one in their "generation". The $n=0$ summand pairs the real charge with the first generation (or primary) image charge to the left. The $n=1$ summand pairs the right primary image with the oppositely charged image charge in the next generation (2nd) to the right. The positive index sums all the image pairs to the right while the negative index sums all the image pairs to the left. As long as we keep this pairing of the image charges intact, this series is, as noted by Kellogg, absolutely and uniformly convergent.

Now we want the potential experienced by a real charge due only to the image charges that it has induced and there are two important modifications of this sum that we need to make. The first is that we must drop part of the first term of the $n=0$ summand. (This would correspond to the self-energy of the electron). The second is that we must introduce a factor of $\frac{1}{2}$ because we are dealing with the interaction of a charge with its own image (energy of assembly). This is why the potential for a point charge in front of a single plane conductor is $-\frac{q}{4x}$ and not $-\frac{q}{2x}$ [3].

We first consider the sum over the negative indices with $c = x$ and $y = z = 0$ and the additional factor of $\frac{1}{2}$ as just noted

$$\frac{1}{2} \sum_{n=-\infty}^{-1} \left(\frac{1}{|-2nL|} - \frac{1}{|2x - 2nL|} \right) \quad (2)$$

which is easily seen to be equivalent to

$$\frac{1}{4L} \sum_{n=1}^{\infty} \left(\frac{1}{n} - \frac{1}{n-a} \right) \quad (3)$$

where $a = x / L$ so that $0 < a < 1$ which implies $|a-n| = n - a$. By an easy manipulation of Equation 5.7.6 of the NIST Handbook [21] we see that this infinite sum is given in closed form by:

$$\sum_{n=1}^{\infty} \left(\frac{1}{n} - \frac{1}{n-a} \right) = \psi(1-a) + \gamma \quad (4)$$

TABLE I. Convergence of the truncated image-charge series toward the closed-form result of Eq. (6).

Terms	Potential
20	-0.6925809270
200	-0.6931409927
2000	-0.6931471181
Eq. (6)	-0.6931471806

where $\psi(z) (= \frac{\Gamma'(z)}{\Gamma(z)})$ is the digamma (or sometimes the Psi) function and γ is Euler-Mascheroni constant (approximately 0.57721). By an analogous reasoning for the positive index case of the Kellogg summation we find

$$\sum_{n=1}^{\infty} \left(\frac{1}{n} - \frac{1}{n+a} \right) = \psi(1+a) + \gamma \quad (5)$$

when we add back in the remaining part of the $n=0$ term (the primary image to the left) and noting the identity $\psi(x+1) - \psi(x) = \frac{1}{x}$ we reach our final destination:

$$V(x) = \frac{1}{4L} [\psi(a) + \psi(1-a) + 2\gamma], \quad a \equiv \frac{x}{L}. \quad (6)$$

Since $\psi(x) \sim -\frac{1}{x}$ for small x , we see immediately that this has the correct limiting form for our problem.

We can also check the image modified Kellogg summation formula against this result. For $x = 0.5$ and $L = 1.0$ we find in Table I that even with 2000 terms we have only achieved 7 correct digits as compared to Eq. (6). So even though this series is convergent, it is very slow to do so. It is instructive to plot the potential of Eq. (6) on an interval alongside the potential obtained from only the first generation of image charges, i.e.

$$V(x) = \frac{1}{4L} \left(-\frac{1}{a} - \frac{1}{1-a} \right) \quad (7)$$

but it is even more interesting to also plot Eq. (7) vs. Eq. (6) when the constant 2γ has been left off Eq. (6)

We see from Fig. 1 that the effect on a real charge due to the infinite series of its image charges in both directions, is largely to add the constant 2γ to a potential made up of only the first generation of images. (Note that the potential depends on ratio $a = \frac{x}{L}$ so that form of the potential stays the same while the maximum tends to zero as L gets large). This screening increases the barrier between the two wells beyond that seen only by the first generation of images. For low energies and large L , we would then expect more charge localization near the walls when compared to only the first generation image charges.

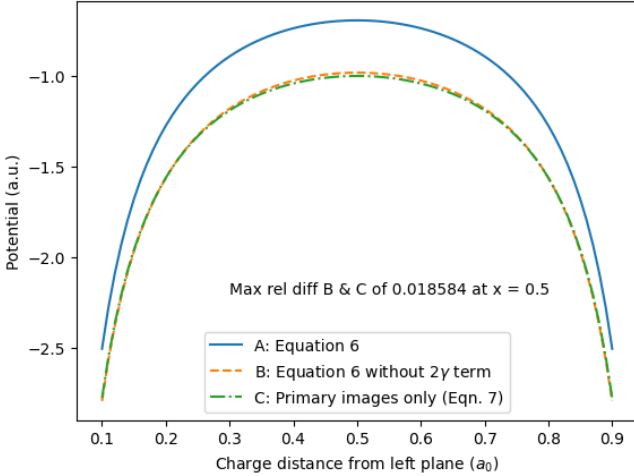


FIG. 1. Comparison of Eq. (6) with and without 2γ vs Eq. (7). $L = 1.0$

III. SOLVING SCHRÖDINGER'S EQUATION WITH A SPECTRAL TECHNIQUE.

In scaled units, the one-dimensional Hamiltonian is now seen to be

$$H(x, L) = -\frac{1}{2} \frac{d^2}{dx^2} + \frac{1}{4L}(\psi(a) + \psi(1-a) + 2\gamma) \quad (8)$$

There are many excellent methods that can be used to solve this one dimensional Schrödinger equation. Among the many we make note of two. First, direct integration of the Schrödinger equation with the Numerov method has a long history [22] and continues to be a popular choice [23]. Second, starting in the 1980's, the Discrete Variable Representation (DVR) has been, and continues to be, widely used for many different problems [24] [25].

Here we will use a DVR-adjacent method known variously in the applied mathematics literature as pseudospectral [26], collocation, discrete ordinates, selected points, or just simply as a spectral method [27] [28].

In using a spectral method, the position variable is considered only on a grid of suitably chosen points (which are usually connected to various families of orthogonal polynomials [27] [28]). Given function values at these points, a spectral differentiation matrix can be constructed, which becomes the core for the kinetic energy operator. One of the key advantages for the spectral method is that potential energy contribution is only needed on these grid points, which are then added to the diagonal of the kinetic energy term to form the Hamiltonian. This is in contrast to the Rayleigh-Ritz procedure, where the matrix elements, which usually result in a dense matrix, must be obtained by integration of the potential energy term between two of the expansion's basis functions. One potential downside to using the spectral method is that we no longer have any guarantees that the calculated values are an upper bound on the true value

of the eigenvalue.

One of the challenges in applying a spectral method is in handling a (semi-)infinite domain. One method is simply to truncate down to a finite interval and examine the eigenvalues for convergence as the interval is increased. This domain truncation can be problematic as noted by Boyd [26]. Another approach is to use Laguerre or Hermite polynomials that are defined over the semi-infinite (Laguerre) or doubly infinite (Hermite) domains. Another approach is to map or scale the infinite interval to finite interval and then use standard spectral methods. Here one must choose a scaling that works well for both the problem and the chosen orthogonal polynomials (which are the implied basis).

However, for this problem, we precisely want a truncated domain. Moreover, since we have Coulomb-like behavior near each boundary, a method that clusters the points near the endpoints of the domain is likely to have better performance than one that does not. This all suggests that the Chebyshev points (which have points clustered near the endpoints proportional to $\frac{1}{\sqrt{1-x^2}}$ as $|x| > 1$ [29] and with the implied 'basis' of Chebyshev polynomials) will have good performance. The final two pieces of the puzzle are a simple linear scaling of the domain and ensuring that the boundary conditions are satisfied. As shown in Chapter 7 of [28], homogeneous Dirichlet boundary conditions are easily enforced by using only the interior Chebyshev points as well as truncating the second order differentiation matrix. The Chebyshev grid points are given by

$$x_j = \cos\left(\frac{j\pi}{M}\right), \quad j = 0, 1, \dots, M. \quad (9)$$

and, just as an example, the off diagonal elements of the differentiation matrix are given by [28]

$$(D_M)_{ij} = \frac{c_i}{c_j} \frac{(-1)^{i+j}}{x_i - x_j}, \quad i \neq j. \quad (10)$$

where $i \neq j$, $i, j = 0, 1, \dots, M$, and $c_i = 2$ for $i = 0, M$ (and $c_i = 1$ otherwise).

Then the spectral Hamiltonian matrix that ensures the boundary conditions are obeyed becomes

$$H_M(L) = -\frac{1}{2} D_{\text{int}}^{(2)} + \text{diag}(V(x_{\text{int}}, L)), \quad (11)$$

where V refers to the potential of Eq. (6), the following dot indicates that this potential is broadcasted over the truncated vector of Chebyshev points, and the `diag` constructs a diagonal matrix from this vector (the actual code is different here for efficiency reasons, see Appendix A). Here we see the great advantage of a spectral method over a Rayleigh-Ritz approach, as noted earlier, we only need to evaluate the potential on a vector of Chebyshev points. Finally, we use the Julia [30] `eigen` function to calculate the eigenvalues and eigenvectors. By default,

TABLE II. Energy levels at large separation ($L = 10000$).

Calculated	Limiting
-0.03125000002884847	-0.03125
-0.031250000028839243	-0.03125
-0.007812500403894916	-0.0078125
-0.007812500403893448	-0.0078125
-0.0034722242129109305	-0.0034722
-0.0034722242129108464	-0.0034722
-0.001953131232235936	-0.001953125
-0.001953131232235714	-0.001953125
-0.0012500151504168003	-0.00125
-0.001250015150416723	-0.00125

TABLE III. Energy levels at $L = 1.0$ ($M = 100$) and the corresponding quantum defect.

N	Calculated	Quantum defect
1	4.0122415062	0.0983071
2	18.467338037	0.0655065
3	42.940196396	0.050169
4	77.341129458	0.0411378
5	121.64356035	0.0351094
6	175.83576914	0.0307642
7	239.91151708	0.0274655
8	313.86707978	0.0248656
9	397.70005311	0.0227576
10	491.40879397	0.02101

Julia uses the LAPACK solvers and specific algorithms can be specified, if desired.

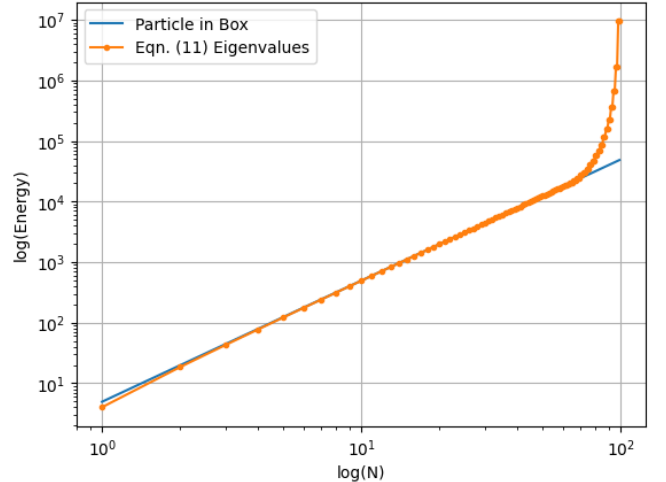
Taking all of these considerations into account results in a remarkably compact program of under 40 lines of Julia code, the entirety of which is reproduced in Appendix A. Since we know what the limiting cases should be, we can easily check that at very large separation we obtain the single plane energy levels for a bound image charge of $-\frac{1}{32n^2}$ [2] only now with a (near) degeneracy of 2. Running the program of Appendix A on an Intel Core i9-9980HK took 2.022 seconds and produced the results of Table II.

IV. RESULTS AND DISCUSSION

In the small L regime, where the PIB-like solutions dominate, the eigenvalues are still close to the ideal PIB values of

$$E_N(L) = \frac{1}{2} \left(\frac{\pi N}{L} \right)^2 \quad (12)$$

as can be seen in Table III

FIG. 2. Log(E) verses Log(N) for $L=1.0$, $M=100$

Here we show the quantum number (N), the calculated energy for $L=1.0$, and the *quantum defect*, that is, the value to subtract from N in order to get the correct energy by using Eq. (12). Note that the quantum defects start out at $\sim 10\%$ but quickly decreases to $\sim 0.2\%$ at $N = 10$.

The visualization of the large N behavior of the energy is done best using a log-log plot of N vs. E . Because of the quadratic dependence on N we see a straight line graph with a slope of 2 in Fig. 2. At small N , the calculated values are seen to differ from the PIB values. At intermediate N , the two energy curves are very close together. At large N we see the eigenvalues of the Hamiltonian matrix (11) rise steeply away from the PIB line and we know that these eigenvalues are not indicative of the solutions to the partial differential equation (8).

Looking at Fig. 2 we might conclude that the eigenvalues are O.K. up to about $N=70$, but that is not the case. A closer look at the $\log(\text{quantum defect})$ vs. $\log(N)$ in Fig. 3 reveals that after gradually decreasing, it starts to fluctuate wildly starting around $N=55$.

This is inline with the rule-of-thumb given in [26] where they note that only $\frac{M}{2}$ of the eigenvalues of the Hamiltonian matrix (11) will be a good approximation to the solutions of (8). This general behavior remains true as the number of Chebyshev grid points, M , is increased.

Turning attention now to the L dependence in the small L regime, we see the $\frac{1}{L^2}$ dependence in Fig. 4. There, the exact PIB eigenvalues are marked for the first few levels at $L = 1, 2$ with a $+$. We see the steep fall off in energy as L grows larger.

If we zoom in on the first two eigenvalues, we see the level splitting as L is varied, as shown in Fig. 5. As L is decreased from a large value, both of these levels decrease in energy due to the image effects of both planes being closer. Unsurprisingly, this is very similar to the level splitting observed in the molecular ion H_2^+ [31].

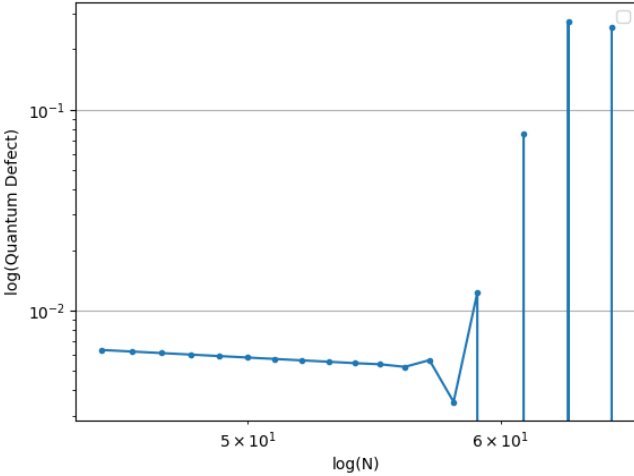


FIG. 3. Log(quantum defect) vs $\log(N)$ for $N=45:65$, $L=1.0$, $M=100$

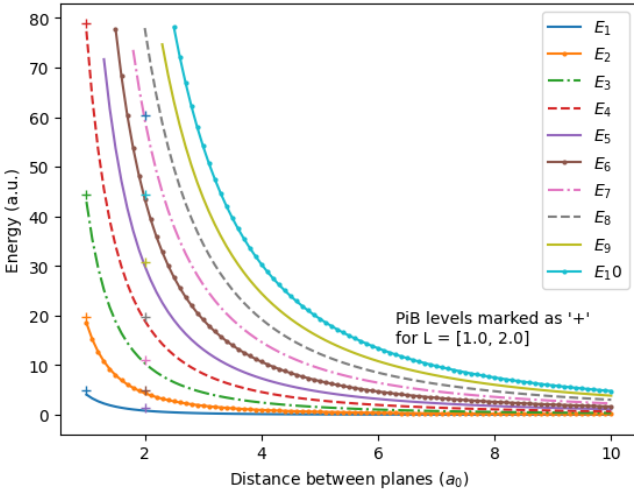


FIG. 4. Energy of the first 10 eigenvalues as function of distance L

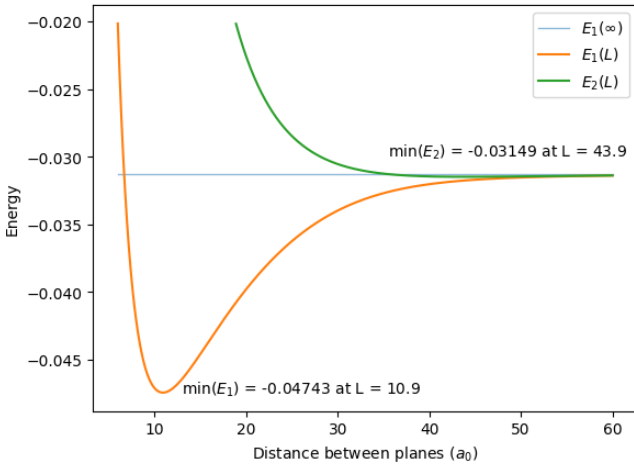


FIG. 5. Energy splitting of first eigenvalue pair as function of distance L

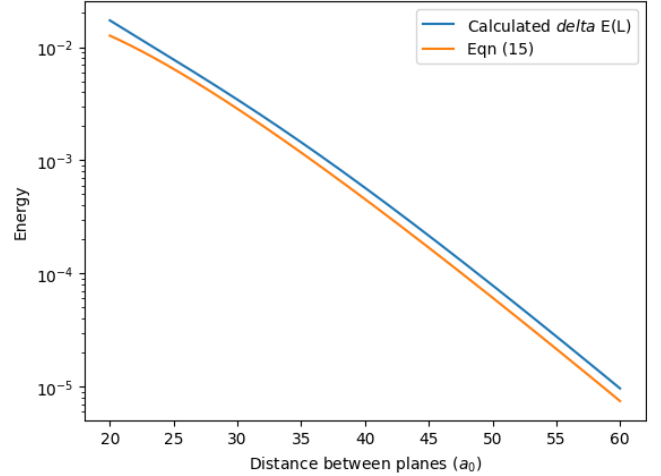


FIG. 6. Delta E for first two states vs. Eq. (15)

The value of the energy splitting can be approximated analytically [32] [33] where they note that this splitting is due to the tunnelling through the central barrier. We start with Eq (2.1) from [33]

$$\Delta E(L) = 2\Psi_0\left(\frac{L}{2}\right)\Psi'_0\left(\frac{L}{2}\right) \quad (13)$$

Here, Ψ_0 refers to the ground state of an electron bound to a single plane. This normalized wavefunction (in a.u.) is given by

$$\Psi_0(x) = \frac{x}{4} \exp\left(-\frac{x}{4}\right) \quad (14)$$

In (13) we have mapped the coordinates to the symmetry point of the interval. Since this splitting is due to tunnelling it makes intuitive sense that it depends on the value of the wavefunction and its derivative at the maximum height of the barrier.

Now (13) is easily seen to be

$$\Delta E(L) = \frac{L}{16} \exp\left(-\frac{L}{4}\right)\left(1 - \frac{L}{8}\right) \quad (15)$$

The prediction of (15) verses the calculated results are shown in a semilog plot in Fig. 6 where it appears that we are only off by a small constant factor.

As the distance between the two planes is increased, the ground state wavefunction transforms from the essentially PIB ground state, where the amplitude is concentrated in the center of the range, to one where the amplitude is concentrated near the planes. Fig. 7 shows the evolution of the first two eigenfunction from the PIB solutions into the symmetric and anti-symmetric combinations of the ground states of two isolated electrons bound by their images.

We note here that as the distance increases much after $100 a_0$ the energy splitting becomes very small and the

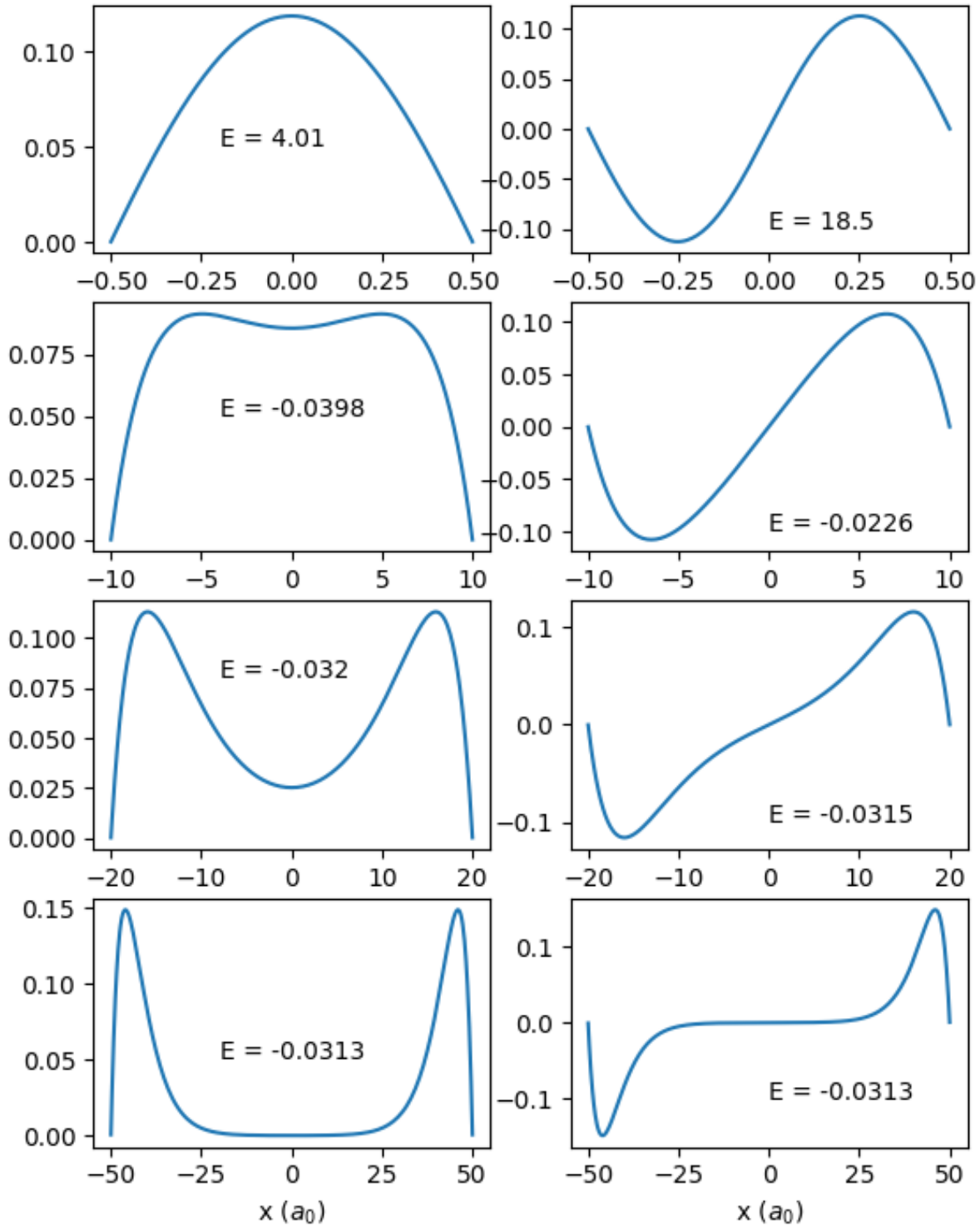


FIG. 7. First pair of eigenfunctions as function of distance L . Rows: $L = [1.0, 20.0, 40.0, 100.0]$ First column: ground state, Second column 1st excited state

returned eigenfunctions for the first two states will be an arbitrary pair of orthogonal functions so that they no longer possess the required even / odd symmetry. However the calculated energy should still remain accurate.

V. CONCLUSION

We have only given a brief outline of the solution and properties of this interesting model problem. We have not fully explained all of the pertinent phenomena and issues and instead rely on the references for much of the deeper theory, which is hoped to be a good guide for the multiple topics touched on here.

Because of the advances in methods (spectral collocation) and software tools (Julia, linear algebra solvers, Matplotlib, etc), this problem becomes accessible to capable undergraduates. Further studies could include examining the splitting of higher excited states, and at large constant L , understanding the transition from an image state to a PIB state as the quantum number increases. Also, calculating and understanding the induced charge density in the planes as a function of L and the quantum number would be interesting. Additionally, using the 'quantum defect' as in Fig. 3 to assess the numerical soundness of the calculated spectrum is appealing because it does not depend on redoing the calculation with increasing number of collocation points. Is there a way to generalize this procedure? Finally, think of your own project, take the code, and run it for yourself!

VI. APPENDIX A

As noted by Trefethen in [28], the calculation of D_2 (the second order differentiation matrix) by squaring D_1 "is not the most stable method, nor the most efficient." We can, for example, use the explicit formulas for D_2 as shown in [34] which reduces the N^3 complexity to N^2 . We can also avoid much of the domain scaling that is in the code below by a more intelligent factoring. We have not done that in this code so that it remains simple and easy to match to the discussion. What is remarkable, is that it still gives excellent results.

```
using Base.MathConstants
using LinearAlgebra
using SpecialFunctions

# Modified from Trefethen's
```

```
# "Spectral Methods in Matlab"
function cheb(M)
    M == 0 && return [], []
    # M+1 points. Use shifted sine for
    # symmetry. See Exercise 2.3 of
    # Trefethen's ATAP
    x = sinpi.((M:-2:-M) ./ 2M)
    c = ones(M+1)
    c[[1,end]] .= 2.0
    c[2:2:end] .*= -1
    X = repeat(x, 1, M+1)
    dX = X - X'
    D = (c * (1 ./ c')) ./ (dX + I)
    D[diagind(D)] .-= sum(D, dims=2)
    return D, x
end

# digamma potential on the interval
# [-L/2, L/2]
function doubleD(x, L)
    a = x / L + 0.5
    return (digamma(a) + digamma(1 - a) +
           2*eulergamma) / 4L
end

# Construct the Hamiltonian
function h_cheb_digamma(;M=10, L=10.0)
    D, x = cheb(M)
    # scale D and x to [-L/2, L/2]
    D .*= (2.0 / L)
    x .*= (L / 2)
    D2 = D^2
    # Set boundary conditions to
    # zero by truncation
    D2 = D2[2:M, 2:M]
    H = -D2 / 2
    H[diagind(H)] .+= doubleD.(x[2:end-1], (L,))
    return H
end

# Check a limiting behavior...
function main()
    vals, vecs = eigen(
        h_cheb_digamma(M=2000, L=10000))
    img_exact = -(1 ./ (1:5) .^ 2) / 32
    for i in 1:10
        println(real(vals[i]), " ",
               img_exact[div(i+1,2)])
    end
end
```

[1] O. D. Kellogg, *Foundations of Potential Theory* (Dover Publications, Inc, 1929).
[2] D. Straub and F. Himpel, Phys. Rev. B **33**,

10.1103/PhysRevB.33.2256 (1986).
[3] P. Echenique, J. Pitarke, E. Chulkov, and V. Silkin, Journal of Electron Spectroscopy and Related Phenomena

126, 10.1016/S0368-2048(02)00150-0 (2002).

[4] A. Michels, J. De Boer, and A. Bijl, *Physica* **4**, 981 (1937).

[5] D. MacMillen and U. Landman, *The Journal of Chemical Physics* **80**, 1691–1702 (1984).

[6] B. Dick, *American Journal of Physics* **41**, 1289 (1973).

[7] B. Dick, *American Journal of Physics* **42**, 1289 (1974).

[8] C. Y. Fong and C. Kittel, *American Journal of Physics* **35**, 10.1119/1.1973741 (1967).

[9] J. D. Jackson, *Classical Electrodynamics* (John Wiley & Sons, Inc., 2001).

[10] J. Pumplin, *American Journal of Physics* **37**, 10.1119/1.1975793 (1969).

[11] M. Glasser, *American Journal of Physics* **38**, 415 (1970).

[12] M. Zahn, *American Journal of Physics* **44**, 1132 (1976).

[13] J. Pleines and S. Mahajan, *American Journal of Physics* **45**, 10.1119/1.11064 (1977).

[14] G. Simon, *American Journal of Physics* **47**, 10.1119/1.11773 (1979).

[15] V. Samedov, *Physics of Atomic Nuclei* **86**, 2634 (2023).

[16] H.-J. Schmidt and T. Brocker, *European Journal of Physics* **46** (2025).

[17] E. Gorbar, V. Gusynin, D. Orieckhov, and B. Shklovskii, *Phys. Rev. B* **109**, 10.1103/PhysRevB.109.165145 (2024).

[18] C. Wagner and F. S. Tautz, *Journal of Condensed Matter Physics* **31** (2019).

[19] M. W. Cole, *Reviews of Modern Physics* **46** (1974).

[20] T. Ando, A. B. Fowler, and F. Stern, *Reviews of Modern Physics* **54** (1982).

[21] F. Olver, A. Olde Daalhuis, D. Lozier, B. Schneider, and R. Boisvert, eds., *NIST Handbook of Mathematical Functions* (NIST and Cambridge University Press, 2010).

[22] J. Cooley, *Mathematics of Computation* **15**, 363 (1961).

[23] M. Purevkhuu and V. Korobov, *Physics of Particles and Nuclei Letters* **18**, 153 (2021).

[24] J. C. Light and T. Carrington Jr., in *Advances in Chemical Physics*, edited by I. Prigogine and S. A. Rice (John Wiley and Sons, 2000) Chap. 4, pp. 263–310.

[25] H. Shi and Z. Sun, *Journal of Mathematical Physics* **66**, 10.1063/5.0270660 (2025).

[26] J. P. Boyd, C. Rangan, and P. Bucksbaum, *Journal of Computational Physics* **188**, 10.1016/S0021-9991(03)00127-X (2003).

[27] J. P. Boyd, *Chebyshev and Fourier Spectral Methods* (Dover Publications, Inc, 2001).

[28] L. N. Trefethen, *Spectral Methods in Matlab* (SIAM, 2000).

[29] L. N. Trefethen, *Approximation Theory and Approximation Practice, Extended Edition* (SIAM, 2019).

[30] J. Bezanson, A. Edelman, S. Karpinski, and V. B. Shah, *SIAM Review* **59**, 10.1137/141000671 (2017).

[31] Olivares-Pilon and A. V. Turbiner, *Annals of Physics* **None**, 10.1016/j.aop.2018.04.021 (2018).

[32] C. Herring, *Reviews of Modern Physics* **134**, 10.1103/RevModPhys.34.631 (1962).

[33] A. Garg, *American Journal of Physics* **68**, 10.1119/1.19458 (2000).

[34] U. Ehrenstein and R. Peyret, *International Journal for Numerical Methods in Fluids* **9**, 10.1002/fld.1650090405 (1989).